

## University of Groningen

### CeFlowBot

Mohanty, Sumit; Paul, Aniruddha; Matos, Pedro M.; Zhang, Jiena; Sikorski, Jakub; Misra, Sarthak

*Published in:*  
Small

*DOI:*  
[10.1002/sml.202105829](https://doi.org/10.1002/sml.202105829)

**IMPORTANT NOTE: You are advised to consult the publisher's version (publisher's PDF) if you wish to cite from it. Please check the document version below.**

*Document Version*  
Publisher's PDF, also known as Version of record

*Publication date:*  
2022

[Link to publication in University of Groningen/UMCG research database](#)

*Citation for published version (APA):*

Mohanty, S., Paul, A., Matos, P. M., Zhang, J., Sikorski, J., & Misra, S. (2022). CeFlowBot: A Biomimetic Flow-Driven Microrobot that Navigates under Magneto-Acoustic Fields. *Small*, 18(9), [2105829]. <https://doi.org/10.1002/sml.202105829>

#### Copyright

Other than for strictly personal use, it is not permitted to download or to forward/distribute the text or part of it without the consent of the author(s) and/or copyright holder(s), unless the work is under an open content license (like Creative Commons).

The publication may also be distributed here under the terms of Article 25fa of the Dutch Copyright Act, indicated by the "Taverne" license. More information can be found on the University of Groningen website: <https://www.rug.nl/library/open-access/self-archiving-pure/taverne-amendment>.

#### Take-down policy

If you believe that this document breaches copyright please contact us providing details, and we will remove access to the work immediately and investigate your claim.

*Downloaded from the University of Groningen/UMCG research database (Pure): <http://www.rug.nl/research/portal>. For technical reasons the number of authors shown on this cover page is limited to 10 maximum.*

# CeFlowBot: A Biomimetic Flow-Driven Microrobot that Navigates under Magneto-Acoustic Fields

Sumit Mohanty,\* Aniruddha Paul, Pedro M. Matos, Jiena Zhang, Jakub Sikorski, and Sarthak Misra\*

Aquatic organisms within the *Cephalopoda* family (e.g., octopuses, squids, cuttlefish) exist that draw the surrounding fluid inside their bodies and expel it in a single jet thrust to swim forward. Like cephalopods, several acoustically powered microsystems share a similar process of fluid expulsion which makes them useful as microfluidic pumps in lab-on-a-chip devices. Herein, an array of acoustically resonant bubbles are employed to mimic this pumping phenomenon inside an untethered microrobot called CeFlowBot. CeFlowBot contains an array of vibrating bubbles that pump fluid through its inner body thereby boosting its propulsion. CeFlowBots are later functionalized with magnetic layers and steered under combined influence of magnetic and acoustic fields. Moreover, acoustic power modulation of CeFlowBots is used to grasp nearby objects and release it in the surrounding workspace. The ability of CeFlowBots to navigate remote environments under magneto-acoustic fields and perform targeted manipulation makes such microrobots useful for clinical applications such as targeted drug delivery. Lastly, an ultrasound imaging system is employed to visualize the motion of CeFlowBots which provides means to deploy such microrobots in hard-to-reach environments inaccessible to optical cameras.


bacterium,<sup>[7]</sup> alga<sup>[8]</sup>). Since most of the above-described organisms are aquatic, their anatomical features precipitate biomimetic approaches to design new microrobots that imitate efficient swimming motion of such organisms.

Within such aquatic creatures, a unique swimming mechanism is demonstrated by organisms (e.g., octopus, squid, cuttlefish) that belong to the *Cephalopoda* family. The cephalopods exhibit a jet-propulsion phenomenon whereby they sequentially inflate and deflate bodies to pump fluid which imparts the necessary thrust to move forward.<sup>[9–14]</sup> This sequential inflation and deflation in cephalopods can be attributed to their elastic bodies which function like a mass-spring system.<sup>[14–16]</sup> These naturally occurring mass-spring resonators have been a motivation to design artificial robotic systems that closely imitate the cephalopod-inspired motion.<sup>[14]</sup> Previously, different fabrication methods (e.g., mold casting,<sup>[9]</sup> 3-D printing,<sup>[10]</sup> shape memory alloys,<sup>[11]</sup> dielectric elastomers,<sup>[13]</sup> elastic membranes<sup>[14])</sup> have produced microrobotic designs that mimic members of the *Cephalopoda* family. Although the aforementioned fabrication methods closely imitate the anatomy of cephalopods up to centimeter scale, their implementation at micro- and nano-scale can be challenging owing to fabrication constraints. Such precise replication of anatomical features at micro- to nano-scale requires multi-step fabrication processes.<sup>[5,17–20]</sup> Specifically, the synthesis of micro-scale movable components that enable

## 1. Introduction

Over the past decade, contactless actuation of microrobots has opened gateways for diverse applications that range from microfluidic technologies, targeted therapy, drug delivery, to microsurgery in remote environments.<sup>[1]</sup> Inspired by nature, many microrobots mimic motion of a myriad of biological organisms from large sea creatures (e.g., octopus,<sup>[2]</sup> stingray,<sup>[3]</sup> jellyfish,<sup>[4]</sup> eel<sup>[5]</sup>), to microorganisms (e.g., sperm cell,<sup>[6]</sup>

S. Mohanty, A. Paul, P. M. Matos, J. Sikorski, S. Misra  
Surgical Robotics Laboratory  
Department of Biomechanical Engineering  
University of Twente  
Enschede, NB 7522, The Netherlands  
E-mail: s.mohanty@utwente.nl; s.misra@utwente.nl

 The ORCID identification number(s) for the author(s) of this article can be found under <https://doi.org/10.1002/smll.202105829>.

© 2021 The Authors. Small published by Wiley-VCH GmbH. This is an open access article under the terms of the Creative Commons Attribution License, which permits use, distribution and reproduction in any medium, provided the original work is properly cited.

DOI: 10.1002/smll.202105829

A. Paul  
School of Electrical Engineering and Computer Science  
KTH Royal Institute of Technology  
Stockholm SE-100 44, Sweden

J. Zhang  
Vascularization Lab  
Department of Biomechanical Engineering  
University of Twente  
Enschede, NB 7522, The Netherlands

S. Misra  
Surgical Robotics Laboratory  
Department of Biomedical Engineering  
University of Groningen and University Medical Center Groningen  
Groningen AV 9713, The Netherlands

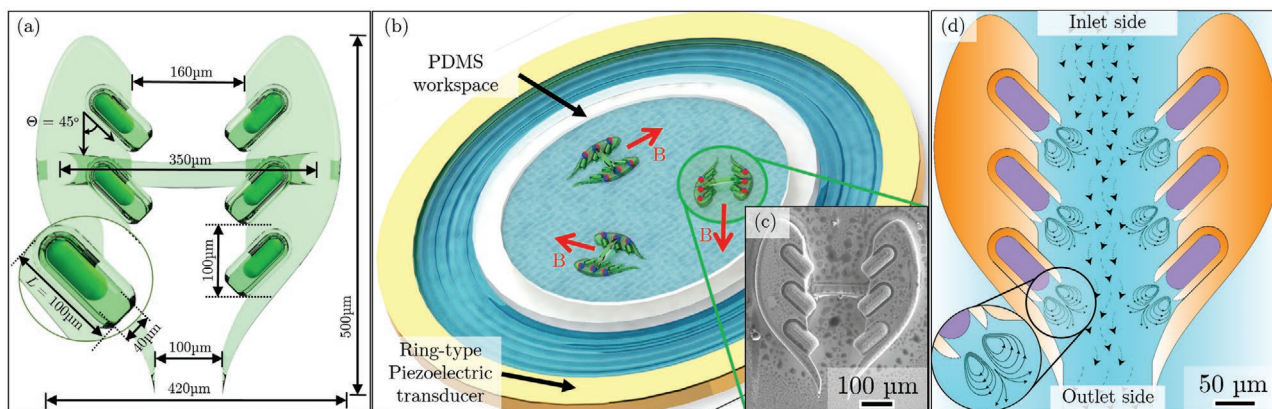


**Figure 1.** a) Schematic of CeFlowBot with the dimensions of its constituent cavity of length,  $L$  (inset), and that of its entire body. The thickness of all the cavities is  $10\ \mu\text{m}$ . b) Illustration of magneto-acoustic actuation of CeFlowBots: An acoustic actuation test-bed comprising an annular piezoelectric transducer (Pz27, Meggitt, Denmark) concentrically bonded to a glass substrate with a polydimethylsiloxane (PDMS)-based ring-shaped workspace on the opposite side. The test-bed is placed at the center of two electromagnets (details in Experimental Section). The arrows (red) show direction of applied magnetic field ( $B$ ) which enables steering of CeFlowBot. c) A micrograph of CeFlowBot showing arrays of cylindrical cavities that trap bubbles. d) The streaming pattern around each of the bubble-entrapped cavities and the resultant flow through the inner channel of CeFlowBots as they are exposed to sound waves while immersed in fluid. The direction of flow in CeFlowBot is from the inlet side to the outlet side akin to a microfluidic channel.

similar kind of body movements as bio-organisms makes their fabrication and actuation difficult.<sup>[4]</sup> In addition, the use of numerous fabrication tools for such multi-step processing also makes the synthesis of such microrobots expensive. This limitation calls for alternative designs of microrobots that replicate the pumping functionality of cephalopods without the need to replicate the precise anatomical features.

Numerous microfluidic devices have been reported with pumping functionality enabled by acoustically induced fluid flow.<sup>[21–24]</sup> A majority of these devices incorporate an array of entrapped bubbles periodically distributed along the microfluidic channels, that vibrate to generate a flow through the channel.<sup>[23,24]</sup> Similar flow fields around a single isolated bubble has also been exploited for actuation of untethered microrobots.<sup>[25–29]</sup> Notably, acoustically resonant bubbles have also been modelled as mass-spring systems which justifies the utility of bubbles as actuators employed in microfluidic pumps and microrobots.<sup>[25,30]</sup> The resonant behavior of compressible bubbles to expend their stored elastic energy has been exploited in many bubble-powered microrobots that optimize propulsion speeds at these resonant frequencies.<sup>[25–30]</sup> Besides such bubble-powered microrobots, many other microrobots utilize vibrating micro-structures for propulsion<sup>[20]</sup> and cargo release.<sup>[5,31]</sup> This ability of microrobots and microfluidic devices to harvest energy from low-intensity sound waves makes their actuation process biocompatible.<sup>[32]</sup> However, a majority of such microrobots rely on vibration of a single bubble which limits their lifetime of actuation. An innovative solution to this limitation is to incorporate arrays of multiple bubbles used inside microfluidic devices as a working principle for actuation of microrobots. Moreover, the resonant amplification in acoustic power due to multiple vibrating bubbles at the same frequency can boost propulsion speeds of microrobots. This bubble-powered acoustic actuation also provides alternate approach to mimic the way cephalopods expend their elastic energy at mechanical resonance. Such a strategy could result in a microrobot design that exhibits a cephalopod-inspired working mechanism while overcoming the

necessity of a cephalopod's design. In this study, we utilize this bubble-powered pumping mechanism in an untethered microrobot where multiple bubbles are actuated in tandem. This pumping ability of our microrobot replicates the jet-propulsion of fluid observed in cephalopods as they deflate their bodies.

We present CeFlowBot, a bubble-powered cephalopod-inspired untethered microrobot capable of locomotion in fluids. CeFlowBot comprises an array of six entrapped air bubbles in its body that vibrate to generate a directional flow through its inner channel (Figure 1a). Further, we synthesize CeFlowBot with magnetic layers which allows it to be steered under uniform magnetic fields while it propels itself under acoustic fields. We utilize this hybrid magneto-acoustic propulsion to demonstrate motion of CeFlowBot in complex trajectories. Next, we demonstrate the ability of CeFlowBot to grasp and release a payload based on power modulation of acoustic fields. Finally, we show motion of CeFlowBot under medical ultrasound (US) imaging system, as means to localize them under clinically relevant scenarios that are hard-to-image with optical cameras.

## 2. Results and Discussions

### 2.1. Design and Fabrication of CeFlowBot

CeFlowBot is composed of two arrays of cylindrical cavities that symmetrically face each other. The two arrays in the microrobot are connected to each other via a bridge to form an open microchannel in between them (Figure 1b,c). The embodied microchannel in CeFlowBot allows the fluid to enter in its body from all sides through a wide inlet as shown in Figure 1d. By contrast, the fluid exits the microchannel through a tapered outlet to facilitate a concentrated flow away from the microrobot (Figure 1d). Further, the cavities in each of the adjacent arrays are tilted ( $45^\circ$ ) with respect to the channel length to facilitate a directional flow of fluid through the channel. CeFlowBots are first 3D micro-printed on a substrate using

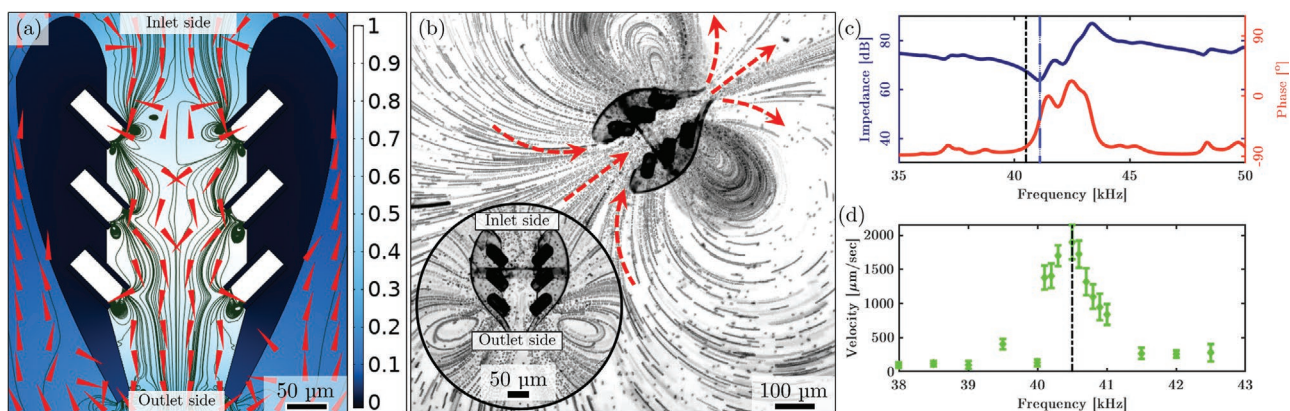


**Figure 2.** a) Numerical simulation of streaming patterns around CeFlowBot at an acoustic frequency of 50 kHz. Color legend represents acoustic pressure (normalized), the red arrows represent fluid particle velocity and black lines represent the streamlines. b) Time-lapse image showing an overlay of streaming motion of polystyrene tracer particles (6 μm diameter, Polysciences Inc., USA) around CeFlowBot when exposed to sound waves. The inset shows time-lapse double-lobed streaming pattern around CeFlowBot over a few periods of acoustic actuation. Both simulated (a) and observed (b) streaming patterns indicate an overall flow of particles (in red) along the same direction, that is, inlet side to outlet side as indicated (Movie S1, Supporting Information). c) Impedance spectrum of piezoelectric transducer used for acoustic actuation experiments. d) Frequency response of CeFlowBots performed at a constant input voltage of 80V<sub>peak-to-peak</sub>. Blue and black lines indicate the resonant frequency of transducer and CeFlowBot, respectively.

Direct Laser Writing (DLW) on an IP-Dip photoresin, and then deposited with metallic layers (Figure S1, Supporting Information). These metallic layers comprised 240 nm of Ni, in order to make CeFlowBot magnetically responsive, followed by 50 nm of Au as an inert protective layer to prevent corrosion of Ni underneath (Figures S2 and S3, Supporting Information). Based on the previous reports of magnetic composition,<sup>[27,28]</sup> a thin layer of Ni (10 nm for ≈10 μm length-scale of microrobot) provides sufficient magnetization volume to impart a soft magnetic character to CeFlowBots. These thin magnetic layers are uniformly deposited using sputtering process and induce an instantaneous magnetic dipole in the CeFlowBots under <10 mT range of magnetic fields. Following the deposition process, these microrobots undergo chemical treatment in order to make their surfaces hydrophobic. Due to this treatment, the microrobots instantaneously trap air bubbles, and thus acoustically responsive, when immersed in their test-bed for actuation (Figure 1d). Lastly, the material selection described above has been previously exploited in microrobots for bio-compatible applications such as their manipulation in cell cultures.<sup>[27]</sup> A detailed account of the cyto-compatibility of the material composition of CeFlowBots is described in Appendix A, Supporting Information. Additional description of the process flow, experimental and imaging setup are provided in the Experimental Section.

## 2.2. Propulsion Mechanism

The air bubbles trapped in the cavities of the CeFlowBot (total size ≈5L), while immersed in water, vibrate in response to incoming sound waves of wavelength (λ). When the trapped bubbles are exposed to sound waves such that λ ≫ L, the vibration of the air-water interface produces counter-rotating fluid fluxes around them. This phenomenon, known as acoustic streaming, results in a net fluid flow directed away from the bubble-entrapped cavities.<sup>[29]</sup> This streaming-induced flow

away from the vibrating end of the cavities results in a reaction force on each cavity, that typically propels most bubble-powered microrobots. In CeFlowBot, the adjacent arrays of tilted cavities function like an acoustically powered microchannel within the microrobot.<sup>[22]</sup> Here, the vibration of these cavities steers an induced flow through the inner body of the CeFlowBot that replicates the pumping action of acoustically powered microchannels. This pumping action compounds the propulsive forces in the microrobot as the fluid enters its inner channel from all sides and exits through the tapered end of the channel. Thus, the streaming-assisted pumping mechanism boosts the bubble-powered propulsion of our microrobot as compared to the untethered microrobots that consist of single entrapped bubbles.

### 2.2.1. Computational and Experimental Verification of Streaming-Induced Flow

Next, we evaluate the induced flow through the inner embodied channel of CeFlowBot based on the computational modeling of its streaming behavior (COMSOL Multiphysics v5.6, COMSOL AB, Sweden). Here, we adopt the simulation environment with a 2D design of the microrobot such that actuation velocities are assigned to the vibrating air–water interface of the cavities.<sup>[29]</sup> We observe an overall net flow through the channel in the direction away from the outlet of the microchannel (Figure 2a). Subsequently, we find that this observation shows the same trend as with the experimental result (Figure 2b). This streaming motion of the particles suggest a net flow through the inner channel of our microrobot alike the flow direction seen in the simulations (Movie S1, Supporting Information). Interestingly, a double-lobed streaming pattern can be seen at the tapered end of the microrobot formed by the flow of particles that exit the channel. This double-lobed streaming indicates a strong flow field comparable to the size of the microrobot which facilitates propulsion of bubble-powered microrobots in the viscous-dominated Stokes regime.<sup>[25,26]</sup>

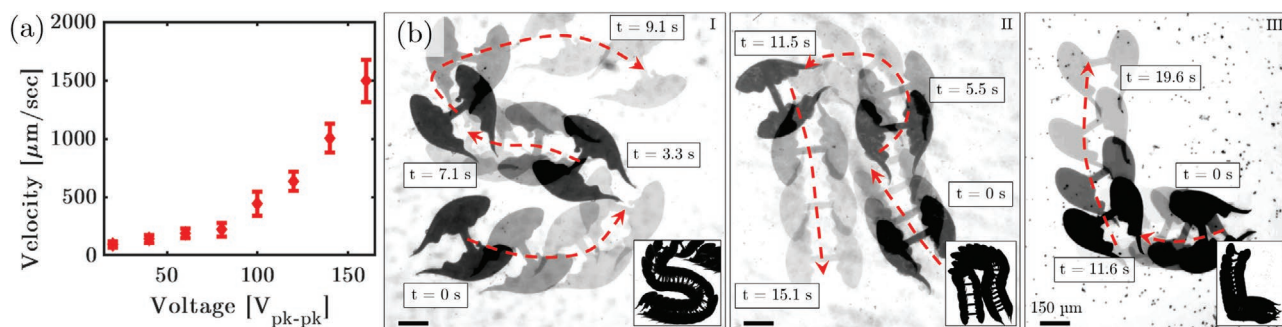


**Figure 3.** a) Velocity characterization CeFlowBots for a power modulation of up to  $160V_{\text{peak-to-peak}}$  at an acoustic frequency of 41kHz (Movie S1, Supporting Information). b) Motion of a CeFlowBot under magneto-acoustic fields showing super-imposed time-stamps of CeFlowBots as they describe the letters I: “S”, II: “R”, and III: “L”, respectively. The insets show all the time-stamps and the overall trajectories in I, II, and III (Movie S2, Supporting Information).

### 2.2.2. Frequency and Power Dependency of CeFlowBots

We identify the acoustic frequencies for actuation of CeFlowBot based on the resonant frequency of its constituent entrapped bubbles. For bubbles entrapped in a cylindrical cavities, the primary acoustic resonant frequency ( $f_r$ ) is expressed as<sup>[32]</sup>

$$f_r = \frac{1}{2\pi} \left( \frac{\kappa_a P_o}{\rho_w L_b (L - L_b)} \right)^{1/2} \quad (1)$$

where  $P_o$ ,  $\kappa_a$ , and  $\rho_w$  denote the ambient pressure in the bubble, adiabatic index of air ( $\leq 1.4$ ), and density of the fluid (water), respectively. Here, the length of all the constituent cavities are the same (i.e.,  $L = 100 \mu\text{m}$ ). However, the length of entrapped bubble ( $L_b$ ) depends on the degree of hydrophobicity in the inner surfaces of the cavities during chemical treatment. We assume that the chemical treatment results in at least  $\geq 50\%$  of the each cavity to be occupied with bubbles (i.e.,  $L_b = 50\text{--}90 \mu\text{m}$ ). Using this range of  $L_b$  in (1), we estimate a frequency range of 35–60 kHz for actuation of our microrobot. Based on this estimate, we choose a piezoelectric transducer (Pz27, Meggitt, Denmark) with a resonant frequency within this range (Figure 2c). Next, we subject our microrobot to acoustic actuation in this range of frequencies to find that it reaches its maximum speed at  $\approx 40.5 \text{ kHz}$  (Figure 2d). Based on (1),  $f_r = 40.5 \text{ kHz}$  corresponds to an average  $L_b = 70 \mu\text{m}$  for all the cavities. Although the precise value of  $L_b$  may vary for each cavity, we attribute any such possible deviations in bubble entrapment to the different degree of hydrophobicity inside each cavity. Finally, we evaluate the performance of the microrobot at the closest integral value of  $f_r$  (i.e., 41 kHz) over a range of power modulation (Figure 3a).

### 2.3. Magneto-Acoustic Actuation

Besides the bubble-powered pumping mechanism, we exploit magnetic steering to demonstrate targeted propulsion of CeFlowBots. A low coercive field strength ( $\approx 90 \text{ Oe}$ ) and high value of saturation magnetization (300 mT) of the magnetic layers enable CeFlowBot to have an induced dipole moment at magnetic fields  $< 10 \text{ mT}$  (Figure S2, Supporting Information).

We first subject CeFlowBot to increasing values of uniform magnetic field (1–10 mT). Although CeFlowBot responds to low magnitude of magnetic fields (1–2 mT), it does not spontaneously align to the direction of applied field. In contrast, we observe CeFlowBot to be more sensitive when steered with magnetic fields of magnitude  $> 4 \text{ mT}$  (Movie S2, Supporting Information). We characterize the steerability of CeFlowBots based on its relative angular misalignment to a range of applied magnetic field magnitudes (Figure S4, Supporting Information). We hereon subject CeFlowBots to the lowest magnitude of applied magnetic field (4 mT) to which it responds with relatively lower misalignment. When this magnetic field is applied, the induced magnetic dipoles cause the long axis of the microrobot to readily align in the direction of the applied field (Figure 1b). Next, magnetic and acoustic actuation are used in tandem to guide the microrobot along specific trajectories. We test this hybrid actuation approach with a square-shaped trajectory that the microrobot describes under the combined magneto-acoustic fields (Movie S2, Supporting Information). Finally, we utilize this approach to guide the propulsion of our microrobot along trajectories that describe the letters “S”, “R”, and “L”, respectively (which stands for Surgical Robotics Laboratory, Figure 3b). The ability of CeFlowBots to maneuver such trajectories makes them suitable for hard-to-navigate environments that often require dexterous direction control like cyclic microchannels or biological vascular pathways.

### 2.4. Applications of CeFlowBot

#### 2.4.1. Localized Payload Delivery

Next, we show the utility of CeFlowBots to perform localized manipulation of nearby micro-agents as payload. For this demonstration, we introduce a star-shaped micro-agent in the acoustic actuation test-bed alongside our microrobots. Here, in addition to the bubble-powered pumping which facilitates microrobot propulsion, these bubbles also exert secondary radiation forces to attract nearby agents.<sup>[27]</sup> We exploit these radiation forces in conjunction with the flow through the inner channel of the microrobot to perform grasp-and-release of a nearby payload (Movie S3, Supporting Information). In this scenario, the microrobot first approaches a nearby star-shaped agent and grasps it

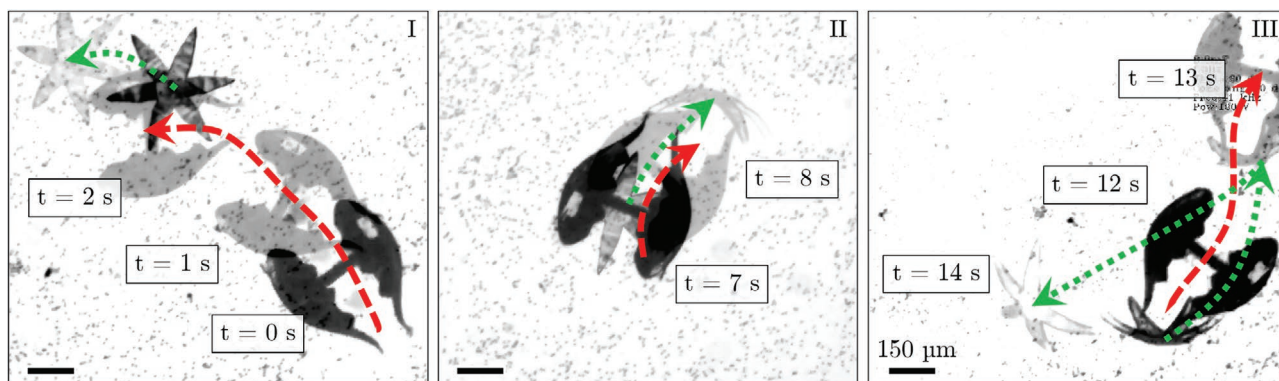


**Figure 4.** Grasp-and-release of a star-shaped micro-agent (indicated with green arrows) as payload using microrobot (indicated with red arrows) showing time-stamps of microrobot approaching the agent with its channel opening (I), agent is pushed toward the channel exit (II), and released with a power-modulated flow (III). Finally, the microrobot escapes post-release ( $t > 13$  s) (Movie S3, Supporting Information).

as the incoming flow fetches the agent toward the microrobot (Figure 4-I). Second, the agent is pushed toward the channel's exit with power modulation of the flow (100 V) (Figure 4-II). Finally, as the acoustic power is increased further (160 V), the microrobot releases the agent and escapes away from it (Figure 4-III). Overall, while radiation forces assist in attracting nearby payloads to the microrobot, the power-modulated pumping mechanism can also play a role in their release near a targeted site.

#### 2.4.2. Combined Actuation and Imaging with Ultrasound Waves

Although the ability to manipulate nearby agents has been demonstrated with many previous untethered microrobots,<sup>[25–28]</sup> their application under remote environments such as *ex vivo*/*in vivo* tissues has been seldom presented. In order to deploy the microrobots in such remote environments, it is required to visualize these microrobots under medical imaging modalities such as US. Since the above-mentioned microrobots<sup>[25–28]</sup> comprise a single microbubble (size  $\approx 10$ – $100$   $\mu\text{m}$ ), they are hard to visualize under commonly available US imaging systems (1–10 MHz). In this regard, designs with arrays of multiple bubbles like CeFlowBot offer an overall larger footprint (i.e., 500  $\mu\text{m}$ ) despite having constituent bubbles of similar size. Thus, such microrobots based on multiple bubbles offer dual advantages: 1) their large footprint for ease of visualization under US imaging system, and 2) constituent microbubbles of length  $< 100$   $\mu\text{m}$  that are small enough to produce high-frequency localized fluid flows. The latter advantage is noteworthy for microrobots that operate in the Stokes regime where the Reynold's number due to bubble-induced streaming is a few orders of magnitude higher than that around the microrobot.<sup>[33]</sup>

Typically, bubble-powered microrobots are actuated in enclosed workspaces where imaging such microrobots with an externally placed US imaging probe could be difficult and noise-prone.<sup>[25–28]</sup> In our experiments, we deploy a CeFlowBot in an enlarged workspace that accommodates a submerged US imaging probe in tandem with an optical camera<sup>[34]</sup> (Figure 5a). Within this workspace, we demonstrate three trials of the microrobot motion visualized using both US and optical imaging systems (Movie S4, Supporting Information). Note that the US imaging system is applied at

its highest frequency of 14 MHz to allow high pixel resolution (details in Experimental Section). A time-lapse sequence of the last trial is presented in Figure 5b,c, where the microrobot travels the furthest (i.e.,  $\approx 4$ – $5$  times its body length from the starting position). The optical images validate the motion observed under the US imaging system; the overall detection of a CeFlowBot in our trials is sufficient to be identified under standalone US imaging. This ease of visibility of CeFlowBot under US imaging system can be useful for clinically relevant scenarios, such as hard-to-access regions of the human body, where optical cameras cannot function.

### 3. Conclusions

In summary, we present a cephalopod-inspired microrobot capable of locomotion under applied magneto-acoustic actuation. CeFlowBot makes use of an array of vibrating bubble-entrapped cavities to mimic the pumping mechanism similar to members of the Cephalopoda family. Compared to other popular microrobots based on vibrating bubbles, CeFlowBot provides a robust solution as its lifetime is not confined to existence of a single bubble. Case in point, a CeFlowBot can function even when a few bubbles within its inner microchannel are dissolved in due course of experiments. Unlike many other bubble-powered microrobots,<sup>[25–28]</sup> the dissolution of a single bubble does not jeopardize the lifetime of a CeFlowBot. The motivation behind the design of CeFlowBots provides a foundation for new acoustic microrobots that capitalize on multiple bubbles for their actuation. Such modular approach to design bubble-powered microrobot offers large footprint of microrobots with almost an order small bubbles as constituent propulsive units. Thus, such a microrobot could retain the dual advantages like ease of handling and visibility due to its large size, and fast motion enabled by high-frequency actuation of small bubbles. These designs of microrobots may extend to millimeter-scale robots with numerous  $\mu\text{m}$ -scale bubble arrays such that each array caters to different functions such as steering or particle manipulation. Further, CeFlowBot can itself be redesigned with a co-axial distribution of such bubble-powered arrays around its inner channel to facilitate its 3-D propulsion.

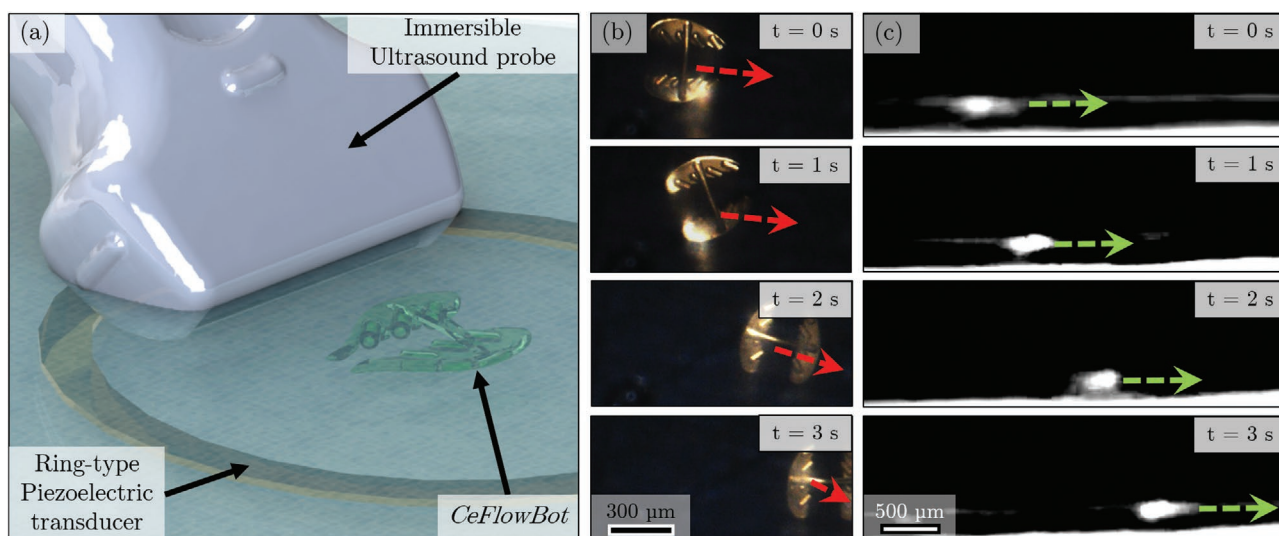


**Figure 5.** a) Schematic of the experimental setup used for ultrasound (US) imaging of acoustically-actuated CeFlowBot (details in Experimental Section). Time-stamps of the motion of CeFlowBot visualized using b) optical and c) US imaging. The arrows indicate direction of motion of the CeFlowBot (Movie S4, Supporting Information).

In this study, we also demonstrate feasibility of CeFlowBot for future clinical applications based on its ability for localized payload manipulation, and its clear distinguishable detection under clinical US imaging system. In terms of payload manipulation, CeFlowBots can be functionalized with chemical receptors to bind and retain the payload over prolonged duration of manipulation.<sup>[28]</sup> With regards to the US imaging experiments, CeFlowBots are more easily detectable under US imaging system in contrast to previously mentioned acoustic microrobots that are powered by a single bubble of length 50–200  $\mu\text{m}$ . In terms of the manipulation ability, CeFlowBot could potentially function as a  $\mu$ -sieve to perform tasks such as filtering, collection and sorting of nearby particles assisted by its tapered inner channel.<sup>[35]</sup> Further, CeFlowBots could be employed in cell cultures to perform targeted manipulation on living cells. Previous studies have suggested magneto-acoustic microrobots with similar composition to be non-cytotoxic in HeLa cell cultures.<sup>[27]</sup> In order to validate biocompatibility of CeFlowBots in such cell cultures, viability tests could be performed in cytotoxicity assays to ensure that the manipulated cells are living post operation. Our future work will address a complete implementation where CeFlowBot navigates to perform such targeted manipulation in biological media such as tissues cultures under US guidance.

#### 4. Experimental Section

**Material and Fabrication Details:** CeFlowBots are monolithic and made up of IP-Dip photoresin (Nanoscribe GmbH, Germany). These microrobots were 3D micro-printed using DLW technique with 25x microscope objective, and DLW was operated with Dip-in-Laser Lithography method. They are printed on an Indium-tin oxide-coated glass substrate in galvo-scanning mode with the laser power of 25 mW and scanning speed of  $4 \times 10^4 \mu\text{msec}^{-1}$ . The design features in the microrobot such as separation between the adjacent arrays and the inter-cavity distance were optimized to the printing area. Particularly, these design metrics (Figure 1d) were tuned such that the overall

footprint of the microrobot fits the DLW field ( $500 \times 500 \mu\text{m}$ ) available for 25x objective. Additionally, the star-shaped micro-agents used for payload delivery are also printed using DLW, with their tip-to-tip length 450  $\mu\text{m}$  and thickness 30  $\mu\text{m}$ . Following the 3D-printing, the microrobots were developed in RER 600 (1-Methoxy-2-propanol acetate) for 25 min and rinsed in isopropyl alcohol for 5 min. Then, the substrate containing the microrobots was baked on a hot plate at 150  $^\circ\text{C}$  for 15 min in order to remove the photoresist residues.

Next, the microrobots were coated with 240 nm layer of Ni followed by 50nm of Au using sputtering process. The saturation magnetization of Ni-coated samples was found to be 26  $\text{emug}^{-1}$  at 0.3 T (Figure S2, Supporting Information). A detailed EDX analysis of the Ni-coated sample and the Ni sputter target is presented in Figure S3, Supporting Information. Prior to the final chemical treatment, the substrate was activated in an oxygen plasma (50 W) for 40 s (Cute, Femto Science Inc, South Korea). Lastly, the substrate was treated with 10  $\mu\text{L}$  of trichlorosilane vapor (PFOCTS, Merck KGaA, Germany) at 55  $^\circ\text{C}$  for 120 min in a closed chamber in order to make them hydrophobic. Following this treatment, the substrate was again baked on a hot plate at 70  $^\circ\text{C}$  for 15 min to get rid of the excessive layers of trichlorosilane. This post-treatment bake prevented the bubbles to slip out of the constituent cavities of CeFlowBots. During the acoustic actuation experiments, the microrobots were immersed in a phosphate-buffered saline (1x-PBS) solution mixed with polystyrene tracer particles (6  $\mu\text{m}$  diameter, Polysciences).

Besides, an additional variant of CeFlowBot with total length 600  $\mu\text{m}$  was printed for experiments under US imaging system. For the experiments under US imaging system, the microrobots with total eight cavities were used, that is, an additional cavity in each side of the array shown in Figure 1d. This design variant was used in order to enlarge its detected footprint relative to acoustic wavelength used for US imaging system (i.e.,  $\approx 105 \mu\text{m}$ ) for imaging frequency of 14 MHz.

**Instrumentation:** Acoustic actuation test-bed was powered with a programmable signal generator (33510B, Keysight, Inc., USA) connected to a 160 V custom-built voltage amplifier (ESyLAB LM3325 8-channel<sup>[56]</sup>) used for acoustic power enhancement. Magnetic actuation was enabled by a set of two orthogonal electromagnets powered by XenusPlus EtherCAT drivers (XE-2-230-20, Copley Controls, USA), providing up to 5 mT of magnetic field.<sup>[7]</sup> The test-bed was mounted on top of an inverted microscope (AxioVert A1, Carl Zeiss AG, Germany) with a CMOS camera (Point Grey Research, Inc., Blackfly GigE vision, pixel size = 3.75  $\mu\text{m}$ ) for

real-time optical imaging. All modules of the system were integrated using a C++ software framework implemented on a Linux Ubuntu 18.04. The image data for both frequency and power modulation experiments were analyzed on custom-made MATLAB (R2021a, Mathworks Inc., USA) scripts. Additionally, US experiments with CeFlowBots were performed under both CMOS camera and an US imaging system (L15 HD Scanner, Clarius Mobile Health, Canada) with an imaging frequency of 14 MHz. The US imaging probe was submerged into acoustic actuation setup (Figure 5a) whereas the optical camera was present at the rear end of the test-bed.

## Supporting Information

Supporting Information is available from the Wiley Online Library or from the author.

## Acknowledgements

This work was supported by funds from The Netherlands Organization for Scientific Research (Innovational Research Incentives Scheme-VIDI: SAMURAI project #14855). The authors would like to thank Nick Helthuis, Remco Sanders, Mike Dikkers, and Harry Bakker for their assistance with the experiments. The authors are grateful to Jeffrey M. McNeill for the insightful discussions throughout the preparation of the manuscript. The authors would also like to thank Venkat Kalpathy Venkiteswaran and Islam S.M. Khalil for reviewing the manuscript.

## Conflict of Interest

The authors declare no conflict of interest.

## Data Availability Statement

The data that support the findings of this study are available in the Supporting Information of this article.

## Keywords

acoustofluidics, biomimicry, magnetic propulsion, microstreaming, microswimmers

Received: September 23, 2021

Revised: November 19, 2021

Published online:

- [1] E. Diller, M. Sitti, *Adv. Funct. Mater.* **2014**, *24*, 4397.
- [2] M. Wehner, R. L. Truby, D. J. Fitzgerald, B. Mosadegh, G. M. Whitesides, J. A. Lewis, R. J. Wood, *Nature* **2016**, *536*, 451.
- [3] S. R. Shin, B. Migliori, B. Miccoli, Y.-C. Li, P. Mostafalu, J. Seo, S. Mandla, A. Enrico, S. Antona, R. Sabarish, T. Zheng, L. Pirrami, K. Zhang, Y. S. Zhang, K.-t. Wan, D. Demarchi, M. R. Dokmeci, A. Khademhosseini, *Adv. Mater.* **2018**, *30*, 1704189.
- [4] Z. Ren, W. Hu, X. Dong, M. Sitti, *Nat. Commun.* **2019**, *10*, 1.
- [5] F. Mushtaq, H. Torlakcik, M. Hoop, B. Jang, F. Carlson, T. Grunow, N. Läubli, A. Ferreira, X.-Z. Chen, B. J. Nelson, S. Pané, *Adv. Funct. Mater.* **2019**, *29*, 1808135.
- [6] V. Magdanz, J. Vivaldi, S. Mohanty, A. Klingner, M. Vendittelli, J. Simmchen, S. Misra, I. S. M. Khalil, *Adv. Sci.* **2021**, *8*, 2004037.
- [7] S. Mohanty, Q. Jin, G. P. Furtado, A. Ghosh, G. Pahapale, I. S. M. Khalil, D. H. Gracias, S. Misra, *Adv. Intell. Syst.* **2020**, *2*, 2000064.
- [8] X. Yan, Q. Zhou, M. Vincent, Y. Deng, J. Yu, J. Xu, T. Xu, T. Tang, L. Bian, Y. X. J. Wang, K. Kostarelos, L. Zhang, *Sci. Robot.* **2017**, *2*, eaq1155.
- [9] F. Giorgio-Serchi, A. Arienti, C. Laschi, *Int J Robot Res.* **2016**, *35*, 1308.
- [10] G. D. Weymouth, V. Subramaniam, M. S. Triantafyllou, *Bioinspiration Biomimetics* **2015**, *10*, 16016.
- [11] Z. Wang, G. Hang, J. Li, Y. Wang, K. Xiao, *Sens. Actuators, A* **2008**, *144*, 354.
- [12] F. Renda, F. Giorgio-Serchi, F. Boyer, C. Laschi, *Bioinspiration Biomimetics* **2015**, *10*, 055005.
- [13] T. Yang, Y. Xiao, Z. Zhang, Y. Liang, G. Li, M. Zhang, S. Li, T. W. Wong, Y. Wang, T. Li, Z. Huang, *Sci. Rep.* **2018**, *8*, 1.
- [14] T. Bujard, F. Giorgio-Serchi, G. D. Weymouth, *Sci. Robot.* **2021**, *6*, eabd2971.
- [15] F. Giorgio-Serchi, G. D. Weymouth, *Biosyst. Birobotics* **2017**, *17*, 37.
- [16] J. M. Gosline, R. E. Shadwick, *Can. J. Zool.* **2011**, *61*, 1421.
- [17] J. Kim, S. E. Chung, S.-E. Choi, H. Lee, J. Kim, S. Kwon, *Nat. Mater.* **2011**, *10*, 747.
- [18] F. Rajabasadi, L. Schwarz, M. Medina-Sánchez, O. G. Schmidt, *Prog. Mater. Sci.* **2021**, *120*, 100808.
- [19] J. Cui, T.-Y. Huang, Z. Luo, P. Testa, H. Gu, X.-Z. Chen, B. J. Nelson, L. J. Heyderman, *Nature* **2019**, *575*, 164.
- [20] D. Ahmed, T. Baasch, B. Jang, S. Pane, J. Dual, B. J. Nelson, *Nano Lett.* **2016**, *16*, 4968.
- [21] P.-H. Huang, N. Nama, Z. Mao, P. Li, J. Rufo, Y. Chen, Y. Xie, C.-H. Wei, L. Wang, T. J. Huang, *Lab Chip* **2014**, *14*, 4319.
- [22] S. Mohanty, U. S. de Cumis, M. Solsona, S. Misra, *AIP Adv.* **2019**, *9*, 035352.
- [23] M. V. Patel, I. A. Nanayakkara, M. G. Simon, A. P. Lee, *Lab Chip* **2014**, *14*, 3860.
- [24] N. Garg, T. M. Westerhof, V. Liu, R. Liu, E. L. Nelson, A. P. Lee, *Microsyst. Nanoeng.* **2018**, *4*, 1.
- [25] N. Bertin, T. A. Spelman, O. Stephan, L. Gredy, M. Bouriau, E. Lauga, P. Marmottant, *Phys. Rev. Appl.* **2015**, *4*, 064012.
- [26] D. Ahmed, C. Dillinger, A. Hong, B. J. Nelson, *Adv. Mater. Technol.* **2017**, *2*, 1700050.
- [27] L. Ren, N. Nama, J. M. McNeill, F. Soto, Z. Yan, W. Liu, W. Wang, J. Wang, T. E. Mallouk, *Sci. Adv.* **2019**, *5*, eaax3084.
- [28] A. Aghakhani, O. Yasa, P. Wrede, M. Sitti, *Proc. Natl. Acad. Sci. USA* **2020**, *117*, 3469.
- [29] S. Mohanty, J. Zhang, J. M. McNeill, T. Kuenen, F. P. Linde, J. Rouwkema, S. Misra, *Sens. Actuators, B* **2021**, *347*, 130589.
- [30] R. J. Dijkink, J. P. V. D. Dennen, C. D. Ohl, A. Prosperetti, *J. Micro-mech. Microeng.* **2006**, *16*, 1653.
- [31] X.-Z. Chen, J.-H. Liu, M. Dong, L. Müller, G. Chatzipiripiridis, C. Hu, A. Terzopoulou, H. Torlakcik, X. Wang, F. Mushtaq, J. Puigmartí-Luis, Q.-D. Shen, B. J. Nelson, S. Pané, *Mater. Horiz.* **2019**, *6*, 1512.
- [32] S. Mohanty, I. S. M. Khalil, S. Misra, *Proc. R. Soc. A* **2020**, *476*, 20200621.
- [33] N. Mobadersany, K. Sarkar, *J. Fluid Mech.* **2019**, *875*, 781.
- [34] Q. Chen, F. W. Liu, Z. Xiao, N. Sharma, S. K. Cho, K. Kim, *IEEE Trans. Biomed. Eng.* **2019**, *66*, 3231.
- [35] M. Kaynak, P. Dirix, M. S. Sakar, *Adv. Sci.* **2020**, *7*, 2001120.
- [36] H. Droogendijk, M. J. De Boer, R. G. Sanders, G. J. Krijnen, *J. Micro-electromech. Syst.* **2015**, *24*, 651.